



Increased liver tumor formation in neutral sphingomyelinase-2-deficient mice

Liansheng Zhong,^{*,†} Ji Na Kong,[§] Michael B. Dinkins,^{**} Silvia Leanhart,^{**} Zhihui Zhu,^{*} Stefka D. Spassieva,^{*} Haiyan Qin,^{*} Hsuan-Pei Lin,^{*} Ahmed Elsherbini,^{*} Rebecca Wang,^{††} Xue Jiang,^{*,§§} Mariana Nikolova-Karakashian,^{*} Guanghu Wang,^{1,*} and Erhard Bieberich^{1,***}

Department of Physiology,^{*} University of Kentucky College of Medicine, Lexington, KY; Department of Bioinformatics,[†] Key Laboratory of Cell Biology of Ministry of Public Health, College of Basic Medical Sciences, China Medical University, Shenyang, People's Republic of China; Department of Biology,[§] Massachusetts Institute of Technology, Cambridge, MA; Department of Neuroscience and Regenerative Medicine,^{**} Medical College of Georgia, Augusta University, Augusta, GA; Johns Hopkins University,^{††} Baltimore, MD; and Rehabilitation Center,^{§§} Shengjing Hospital of China Medical University, Shenyang, People's Republic of China

Abstract Sphingolipids are key signaling lipids in cancer. Genome-wide studies have identified neutral SMase-2 (nSMase2), an enzyme generating ceramide from SM, as a potential repressor for hepatocellular carcinoma. However, little is known about the sphingolipids regulated by nSMase2 and their roles in liver tumor development. We discovered growth of spontaneous liver tumors in 27.3% (9 of 33) of aged male nSMase2-deficient (*fro/fro*) mice. Lipidomics analysis showed a marked increase of SM in the tumor. Unexpectedly, tumor tissues presented with more than a 7-fold increase of C₁₆-ceramide, concurrent with upregulation of ceramide synthase 5. The *fro/fro* liver tumor, but not adjacent tissue, exhibited substantial accumulation of lipid droplets, suggesting that nSMase2 deficiency is associated with tumor growth and increased neutral lipid generation in the tumor. Tumor tissue expressed significantly increased levels of CD133 and EpCAM mRNA, two markers of liver cancer stem-like cells (CSCs) and higher levels of phosphorylated signal transducer and activator of transcription 3, an essential regulator of stemness. CD133(+) cells showed strong labeling for SM and ceramide. **In conclusion, these results suggest that SMase-2 deficiency plays a role in the survival or proliferation of CSCs, leading to spontaneous tumors, which is associated with tumor-specific effects on lipid homeostasis.**—Zhong, L., J. N. Kong, M. B. Dinkins, S. Leanhart, Z. Zhu, S. D. Spassieva, H. Qin, H-P. Lin, A. Elsherbini, R. Wang, X. Jiang, M. Nikolova-Karakashian, G. Wang, and E. Bieberich. **Increased liver tumor formation in neutral sphingomyelinase-2-deficient mice.** *J. Lipid Res.* 2018. 59: 795–804.

Supplementary key words sphingolipids • lipid • ceramide • lipidomics • sphingomyelin phosphodiesterase 3 • cancer stem-like cells • sphingomyelin • ceramide synthase 5

This work was supported by National Institutes of Health Grants R01AG034389 and R01NS095215 (E.B.) and American Lung Association Grant RG-351396 (G.W.). The content is solely the responsibility of the authors and does not necessarily represent the official views of the National Institutes of Health. The authors do not claim any conflicts of interest.

Manuscript received 25 September 2017 and in revised form 26 February 2018.

Published, JLR Papers in Press, March 22, 2018

DOI <https://doi.org/10.1194/jlr.M080879>

Copyright © 2018 by the American Society for Biochemistry and Molecular Biology, Inc.

This article is available online at <http://www.jlr.org>

Sphingolipids, especially ceramide, sphingosine, and sphingosine-1-phosphate, play essential roles in cell signaling (1–5). They are modulators of various aspects of biology and pathology, including aging and cancer. In cancer, sphingolipids regulate tumor initiation, progression, metastasis, and drug resistance (1, 3, 5–9). Excess ceramide leads to cancer cell death, reduced growth, and senescence, and may serve as a real-time predictive marker for radiation treatment response (6, 7, 9, 10). On the other hand, sphingosine-1-phosphate promotes inflammation, metastasis, proliferation, vasculogenesis, and drug resistance (4, 5, 8, 11).

Mainly three pathways generate ceramide, namely the de novo pathway, the salvage pathway, and the SM cycle (12–14). Several enzymes are involved in the SM cycle, including the SM synthases (SMSs) (SMS1 and SMS2) that catalyze the conversion of ceramide to SM, and several SMases that hydrolyze SM to generate ceramide (13, 15–18). Acid SMase, encoded by SM phosphodiesterase (*Smpd1*), is a lysosomal enzyme the deficiency of which is associated with Niemann-Pick disease (19, 20). Four mammalian neutral SMases (nSMases) have been identified so far, among which nSMase2 (encoded by *Smpd3*) appears to be the predominant nSMase in various tissues and associated pathophysiology (12, 15, 21). Mice deficient in nSMase2 have multiple developmental defects, including dwarfism and delayed puberty, attributed to hypothalamic pituitary deficiency (16–18). nSMase2 is implicated in diverse cellular

Abbreviations: CerS, ceramide synthase; CSC, cancer stem-like cell; dh, dihydro; HCC, hepatocellular carcinoma; IS, internal standard; LD, lipid droplet; nSMase2, neutral SMase-2; ORO, Oil Red O; pStat3, phosphorylated signal transducer and activator of transcription 3; qPCR, quantitative PCR; *Smpd*, SM phosphodiesterase; SMS, SM synthase; Stat3, signal transducer and activator of transcription 3; tStat3, total signal transducer and activator of transcription 3.

¹To whom correspondence should be addressed.
e-mail: Guanghu.wang@uky.edu (G.W.);
erhard.bieberich@uky.edu (E.B.)

functions, including inflammation and pathophysiology of pulmonary, circulatory, cardiac, and neurological systems (15). It is also implicated in cancers, such as leukemia, breast cancer, and liver cancer (22, 23). A recent genome-wide study indicates that *Smpd3* is a potential repressor of hepatocellular carcinoma (HCC) (24).

Sphingolipids play essential roles in stem cell and cancer stem-like cell (CSC) biology (2, 25–29). CSCs, also termed cancer-initiating cells or tumor-initiating cells, are a subpopulation of cells in the tumor that possess stem cell characteristics (30, 31). They are derived from either reactivation of dormant progenitor cells or dedifferentiation of somatic cells (30–32). Mounting evidence has demonstrated that CSCs contribute significantly to tumor initiation, metastasis, treatment resistance, and relapse in many cancer types, including liver cancer (30, 31). Thus, identifying and targeting CSCs is a promising new strategy for cancer therapy (33). Signal transducer and activator of transcription 3 (Stat3) is a key transcription factor in maintaining mouse embryonic stem cell self-renewal and CSC stemness (34–37). Stat3 is phosphorylated and activated by Janus kinases (30). The activated Stat3 translocates into the nucleus and binds to promoters of stemness genes, including the liver CSC marker protein, CD133, leading to their expression (30, 35).

We report here the potential function of sphingolipids in liver tumor development using the nSMase2-deficient (*fragilitas ossium*, *fro/fro*) mouse line (38, 39). This mouse line was discovered in a random-bred stock of mice after treatment with the chemical mutagen, tris(1-aziridinyl) phosphine-sulphine (40), which caused a deletion in the *Smpd3* gene leading to loss of enzyme activity (38). These mice show similar phenotypes as nSMase2 knockout mice generated through gene-targeting approaches (16–18). In our study, liver tumors were observed in 27.3% of aged male *fro/fro* mice (9 of 33), accompanied by increased proliferation and apoptosis. Lipidomics studies demonstrate a marked increase of C₁₆-SM, C₁₈-SM, C_{24:1}-SM, C₁₆-ceramide, and dihydro (dh)C₁₆-ceramide in the tumor tissue. The number of CSCs was increased in *fro/fro* liver tumors, as determined by quantitative (q)PCR and immunocytochemistry of marker genes CD133 and/or EpCAM. Interestingly, CD133(+) cells were labeled for high levels of SM and ceramide. Furthermore, *fro/fro* liver tumors exhibited a significant increase of ceramide synthase (CerS)5 expression and lipid droplet (LD) content, suggesting that the lack of nSMase2 was associated with a compensatory upregulation of sphingolipid and neutral lipid synthesis, which may play a role in CSC proliferation/survival and tumor formation in the *fro/fro* mouse.

MATERIALS AND METHODS

Materials

Oil Red O (ORO), propylene glycol, and fluoroshield supplemented with DAPI were from Sigma-Aldrich (St. Louis, MO). Anti-Ki67 was from Novocastra (Buffalo Grove, IL). Lysenin and anti-lysenin antibody were from Peptide Institute, Inc. (Osaka, Japan). Anti-CD133 was from EMD Millipore (Billerica, MA).

Anti-phosphorylated (p)Stat3 and anti-total (t)Stat3 were from Cell Signaling Technology (Danvers, MA). Anti-ceramide rabbit IgG was generated in our laboratory as described previously (41). Fluorophore-conjugated secondary antibodies were from Jackson ImmunoResearch Laboratories (West Grove, PA). The in situ TUNEL fluorescence staining kit was from Roche (Indianapolis, IN).

Animals

The nSMase2-deficient (*fro/fro*) mouse line (C3H and C57Bl6 mixed background), carrying a deletion in the *Smpd3* gene, was a gift from Dr. Christophe Poirier, Indiana University, Indianapolis, IN (38, 39). These mice were maintained in the Laboratory Animal Service facility of the Medical College of Georgia at Augusta University according to the National Institutes of Health's *Guide for the Care and Use of Laboratory Animals*. All procedures were approved by the Augusta University Institutional Animal Care and Use Committee.

Methods

Tissue collection. Tumor and adjacent normal tissues were collected immediately after surgery by either snap-freeze in -80°C or fixation with 4% PFA. Frozen tissues were never allowed to thaw after initial freezing until used for further experiments. Fixed tissues were either embedded in optimal cutting temperature medium or paraffin for sectioning. H&E staining and RNA analysis were used for quality control of the integrity of the samples.

Histology, immunohistochemistry, and confocal laser microscopy. For histology studies, paraffin-embedded tissues were sectioned into 10 μm slices and stained by H&E in the Electron Microscopy and Histology Core Laboratory at Augusta University (directed by Dr. Sylvia B. Smith). For immunohistochemistry, frozen or paraffin sections were immunolabeled with the antibodies listed and images taken using a Zeiss LSM 510 upright or a Zeiss LSM 780 inverted confocal laser scanning microscope equipped with a two photon argon laser at 488 nm (Cy2), 543 nm (Cy3), and 633 nm (Cy5, Alexa Fluor 647), respectively. LSM 510 Meta 3.2 software was used for image acquisition and processing. Samples labeled with antibodies against lipids were only PFA-fixed and frozen for cryosectioning. Images obtained with secondary antibodies were only used as negative controls to correct for background intensity of a particular laser channel. Antigen-specific immunolabeling was quantified by counting cells that showed signals 2-fold or more above background fluorescence. The percentage of Ki67- and TUNEL-positive cells was counted at $\times 400$ magnification in at least five random fields where tumors existed.

ORO staining. Fixed frozen sections were washed with distilled water. Excess water was drained and depleted by rinsing twice using propylene glycol. ORO was applied and incubated for 7 min at 60°C . Specimens were destained with 85% propylene glycol, rinsed in distilled water, and counterstained using hematoxylin. After sufficient washing with water, specimens were mounted with aqueous mounting media and microscopic images taken using an epifluorescence microscope.

RNA extraction, RT-PCR, and qPCR. RNA was extracted using the TriZol reagent (Invitrogen). First strand cDNA was generated by the iScript cDNA synthesis kit (Bio-Rad, Hercules, CA). Real-time qPCR was performed using SYBR green/Rox qPCR master mix on the CFX96 Touch real-time system (Bio-Rad). The primers for qPCR were: mCerS5-forward, TAGAGAGCAGCTGAGAGGAAGAAGA; mCerS5-reverse, GAACCCAGAGTCTCAAGAGC-CATGGC; mCD133-forward, CAGCAATCACTGAAATTTGTG; mCD133-reverse, ACATCCTCTGAATCCATCCTG; mEpCAM-forward, TATTTTGAAAAAGATGTGAAG; mEpCAM-reverse, ATTAAGCTCTCTGTGGATCTC.

Sphingolipid measurement. Liver tissues were analyzed at the Lipidomics Core of the Medical University of South Carolina

TABLE 1. Incidents of liver tumors in *fro/fro* mice

| Genotype | Gender | Age (months) | Number of Mice with Tumor | Total Mouse Number | Tumor Ratio (%) |
|----------------|--------|--------------|---------------------------|--------------------|-----------------|
| <i>fro/+</i> | Male | 16–24 | 0 | 21 | 0 |
| <i>fro/fro</i> | Female | 16–24 | 0 | 31 | 0 |
| <i>fro/fro</i> | Male | 16–24 | 9 | 33 | 27.3 |

according to published protocols on a Thermo Fisher TSQ Quantum triple quadrupole mass spectrometer, operating in a multiple reaction monitoring positive ionization mode (42). Briefly, similar amounts of tissue were homogenized, protein concentration determined, aliquots of the homogenates equivalent to 1.5 mg protein fortified with internal standards (ISs), and lipids from the fortified homogenates extracted twice with 2 ml ethyl acetate, isopropanol, and water (60:30:10 v/v/v) solvent. Lipid extracts were evaporated and reconstituted in 150 μ l of 1 mM ammonium formate in 0.2% formic acid in methanol before being subjected to LC-MS/MS on the HP1100/TSQ Quantum LC-MS/MS system. The samples were gradient-eluted from the BDS Hypersil C8, 150 \times 3.2 mm, 3 μ m particle size column, with a 1.0 mM methanolic ammonium formate per 2 mM aqueous ammonium formate mobile

phase system. Peaks corresponding to the target analytes and ISs were collected and processed using the Xcalibur software system. Quantitative analysis was based on the calibration curves generated by spiking an artificial matrix with the known amounts of the target analyte synthetic standards and an equal amount of the ISs. The target analyte/IS peak area ratios were plotted against analyte concentration. The target analyte/IS peak area ratios from the samples were similarly normalized to their respective IS and compared with the calibration curves using a linear regression model. Results were normalized to lipid phosphate.

Statistics. The statistical significance was calculated using Student's *t*-test with Excel or one-way ANOVA and Tukey's post hoc test with GraphPad Prism. $P < 0.05$ was considered significant.

RESULTS

Aged *fro/fro* male mice show liver tumors

To determine a potential involvement of nSMase2 and sphingolipids in hepatic cancer, we analyzed liver tissue in

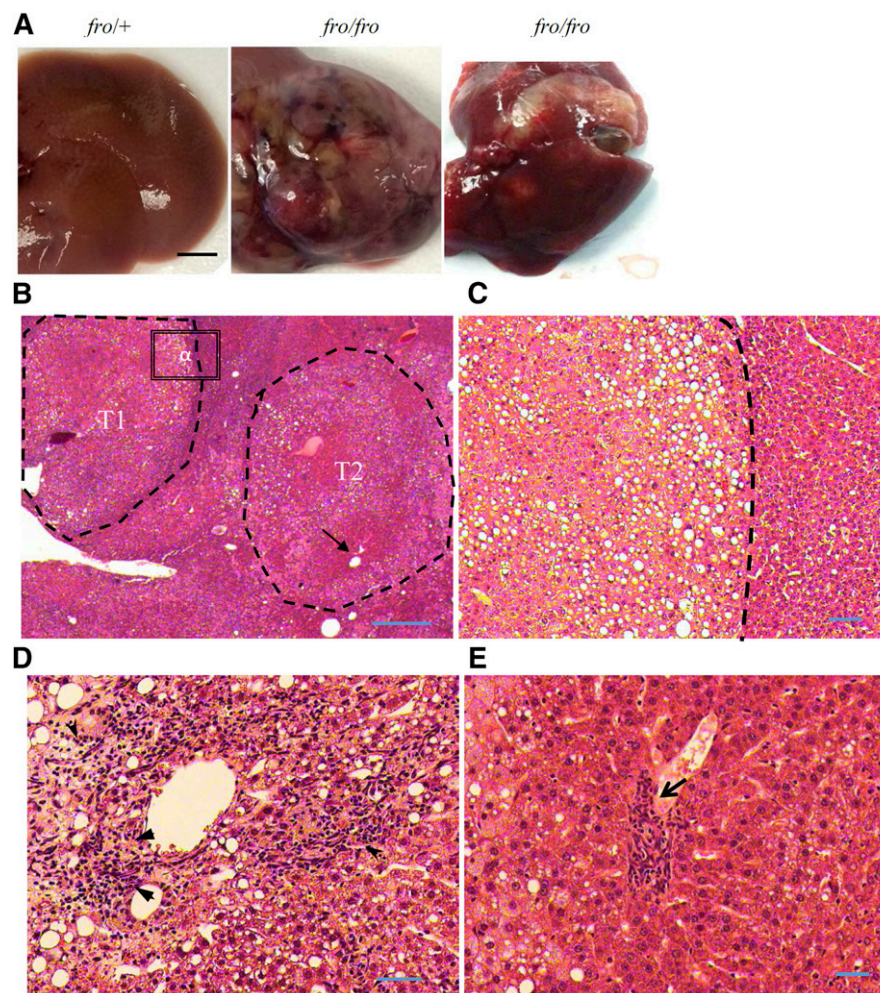


Fig. 1. Gross and microscopic features of liver tumors in *fro/fro* mice. A: Tumors were observed in aged male *fro/fro* mouse livers. One age-matched *fro/+* control (left) and two tumors are shown (right). These tumors contained heterogeneous nodules sized from 0.1 to 5 mm. The color of many nodules was pale, suggestive of focal fat accumulation. Scale bar = 2 mm. B: H&E staining showed two well-defined proliferation nodules within the tumor. Scale bar = 200 μ m. C: Higher magnification of inset α in B. The tumor contains large and vacuolated hepatocytes (left). Liver parenchyma was pushed to the side (right). Scale bar = 10 μ m. D, E: Profound cell hyperplasia (arrowheads) (D) and lymphocyte infiltration (arrows) (E) in the tumor. Scale bars = 50 μ m.

aged *fro/fro* mice (38, 39). Spontaneous hepatic tumors were observed in 9 out of 33 (27.3%) aged (18–24 months old) male *fro/fro* mouse livers (38) (Table 1, Fig. 1A). The phenomenon appeared to be age- and sex-dependent because no tumors were detected in young (less than 10 months old) or in age-matched female (0 of 31) *fro/fro* mice (Table 1). The incidence in aged-matched male controls (*fro/+*) was also 0% (0 of 21) (Table 1). The liver tumors contained heterogeneous proliferation nodules sized 0.1–5 mm in diameter (Fig. 1A). The color of many nodules was pale, suggestive of focal fat accumulation (Fig. 1A).

H&E staining of the tumor sections revealed many well-defined proliferation nodules of varying sizes (T1 and T2, Fig. 1B). Higher magnification of the inset α in nodule T1 indicated a clear boundary between the tumor tissue and liver parenchyma (Fig. 1C). The hepatocytes within the tumor showed enlarged and vacuolated cytoplasm, suggesting fat buildup (Fig. 1C). Pronounced cell hyperplasia (arrowheads, Fig. 1D) and penetration of lymphocytes along the portal vein (arrow, Fig. 1E) were observed within the tumor.

Enhanced proliferation and apoptosis in *fro/fro* liver tumors

Dysregulated cell proliferation and death is a hallmark of cancer (43). We detected the rate of cell proliferation and death in the *fro/fro* liver tumors. The number of Ki67-positive cells was markedly increased in the tumors when compared with normal adjacent tissues (Fig. 2A, C), indicating that cell proliferation was enhanced. On the other hand, the number of TUNEL-positive cells was also markedly increased, indicating augmented apoptosis (Fig. 2B, C). These results are consistent with clinical findings that, although evasion of cell death pathways is a major attribute of cancer, as tumor cells grow and exhaust the nutritional supply from blood circulation, dead cells remain a common feature of many malignancies (44, 45).

Increased number of CSCs in *fro/fro* liver tumors

CSCs contribute to liver carcinogenesis (46–48). The *fro/fro* liver tumors contained pockets of proliferating cells (Figs. 1D, 2A), which could be due to the existence of CSCs. To dissect the cell source of tumor formation, we tested for the presence of CSCs in *fro/fro* liver tumors. RT-PCR and qPCR results showed that the message levels of CD133 and EpCAM, two markers of liver CSCs (30, 35), were increased by 15- and 54-fold, respectively, in *fro/fro* liver tumors when compared with adjacent normal tissues (Fig. 3A, B).

The IL6/JAK/Stat3 pathway is essential for stem cell pluripotency and CSC stemness (34–37). Sphingolipids have been shown to regulate multiple pluripotency pathways, including the Akt/GSK-3 β and IL6/JAK/Stat3 pathways (3, 49–51). We tested to determine whether nSMase2 deficiency in *fro/fro* mice had an effect on these pathways. Western blot analysis showed that the pStat3 level when normalized to tStat3 was significantly increased in *fro/fro* liver tumors as compared with adjacent normal tissue, indicating that the IL6/JAK/Stat3 pathway was activated in *fro/fro* liver tumors (Fig. 3C, D). However, the Akt/GSK-3 β pathway was not activated (not shown). To further elucidate that

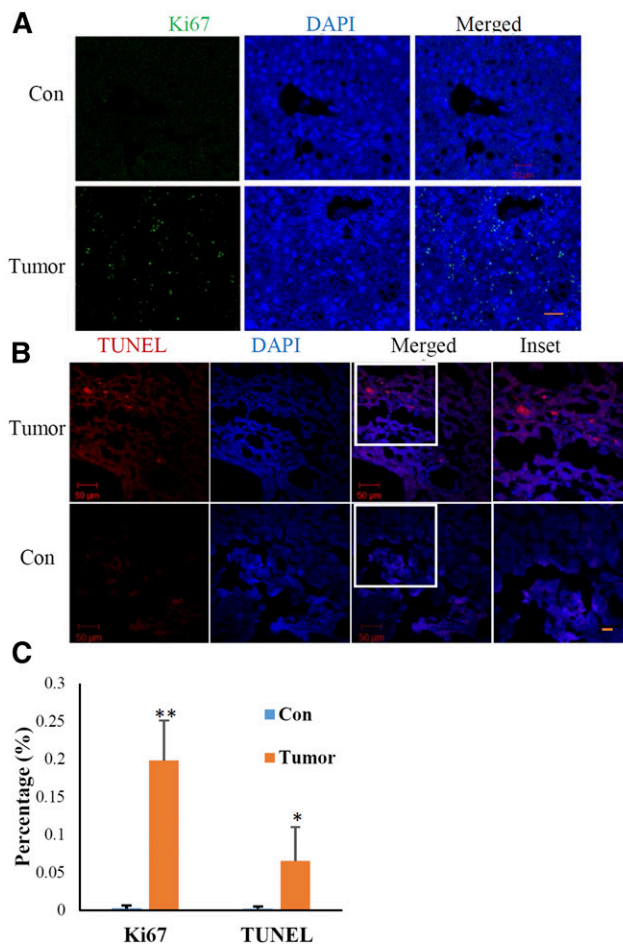


Fig. 2. Increased proliferation and cell death in *fro/fro* liver tumors. A: Proliferation was increased in *fro/fro* liver tumors as shown by Ki67 labeling (green). Con, *fro/+* liver tissue; Tumor, *fro/fro* tumor. Scale bar = 20 μ m. B: Apoptosis was augmented in *fro/fro* liver tumors, as shown by TUNEL staining (red). Scale bars = 50 μ m. C: Quantification of Ki67- and TUNEL-positive cells in A and B. N = 5. * $P < 0.05$, ** $P < 0.01$.

CSCs were increased in *fro/fro* liver tumors, we colabeled for CD133 and pStat3. Figure 3E shows that there were pockets of CD133(+) CSCs in *fro/fro* liver, which colabeled exclusively with pStat3, indicating that the CD133(+) cells were pluripotent (Fig. 3E). We could not detect CD133(+) or pStat3(+) cells in control (*fro/+*) liver tissue (Fig. 3E).

Aberrant sphingolipid profile in *fro/fro* liver tumors

To understand the mechanism of liver tumor formation related to sphingolipids, we analyzed the alteration of the sphingolipid profile caused by nSMase2 deficiency. nSMase2 catalyzes SM hydrolysis to generate ceramide. Consistently, fibroblasts from *fro/fro* mice showed accumulation of SM (52). Lipidomics (LC-MS/MS) data indicated that the major SM species in the liver, C₁₆-, C₂₂-, C₂₄-, and C_{24:1}-SM, were slightly upregulated in normal adjacent *fro/fro* liver tissue when compared with age-matched *fro/+* controls (Fig. 4A and not shown). Although consistent with a previous report (52), the differences were not statistically significant. In contrast, in the *fro/fro* tumors, the levels of C₁₆- and C₁₈-SM and total SM were all significantly increased when compared with normal adjacent liver tissues or to age-matched

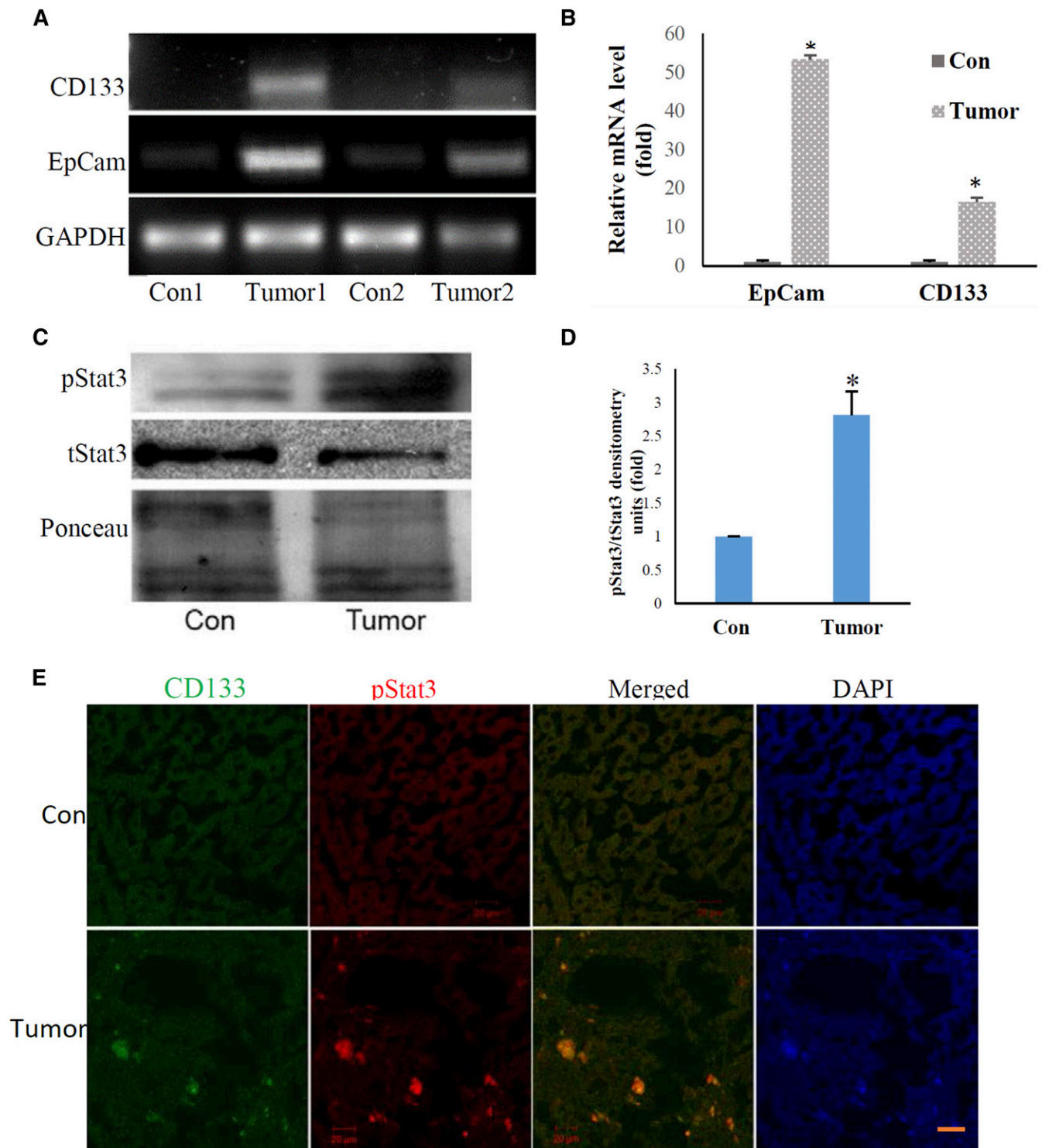


Fig. 3. CSCs in *fro/fro* liver tumors. A, B: The levels of liver CSC markers CD133 and EpCAM were significantly increased in *fro/fro* liver tumors shown by RT-PCR (A) and qPCR (B). Con, *fro/+* liver tissue; Tumor, *fro/fro* tumor. C, D: The level of pStat3 was significantly increased in *fro/fro* liver tumors, as shown by Western blot (C) and densitometric quantification (D). E: CD133(+) (green) cells were positive for pStat3 (red). Scale bar = 20 μ m.

fro/+ controls (Fig. 4A). In particular, the level of C₁₆-SM was increased by more than 4-fold (Fig. 4A).

Surprisingly, total ceramide content was also significantly increased in *fro/fro* liver tumors when compared with normal adjacent liver tissues or age-matched *fro/+* controls (Fig. 4B). The levels of C₁₆ ceramide and dhC₁₆ ceramide, especially, were increased by more than 7-fold (Fig. 4B),

although they were not dominant ceramide species in the liver (not shown). In addition, the levels of dhC₁₆- and C_{24:1}-ceramide were significantly higher in normal adjacent tissue of *fro/fro* liver than control *fro/+* liver (Fig. 4B). The level of C₁₆-ceramide was increased in *fro/fro* non-tumor tissue, but the difference was not statistically significant when compared with *fro/+* controls (not shown).

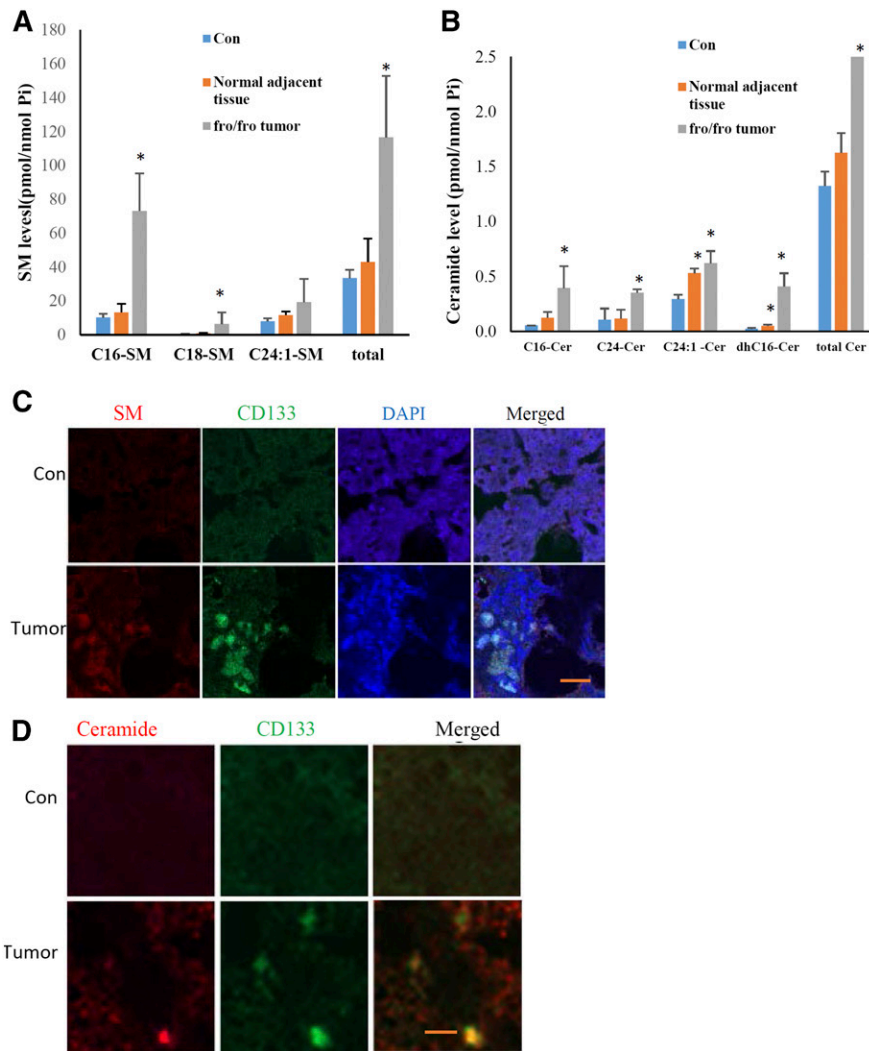


Fig. 4. Aberrant sphingolipid metabolism in *fro/fro* liver tumors. **A:** Lipidomics analyses showed that C_{16} , C_{18} , and total SM were significantly increased in *fro/fro* liver tumors. Control animal was *fro/+* liver; normal adjacent tissue was from *fro/fro* animals that had tumors. $N = 2$. $*$, $P < 0.05$. **B:** Lipidomics analyses showed that the levels of ceramide, especially C_{16} , C_{24} , $C_{24:1}$, and total ceramide were increased in *fro/fro* liver tumors. $N = 2$. $*$, $P < 0.05$. **C:** Coimmunolabeling of CD133 and SM. Scale bar = 20 μm . **D:** Coimmunolabeling of CD133 and ceramide. Scale bar = 20 μm .

To investigate whether accumulation of SM and ceramide were associated with CSC formation, we colabeled liver tissues with antibodies against CD133, ceramide, and SM (pre-incubated by lysenin). CD133 reactivity was located in cells that showed strong labeling of SM (Fig. 4C) and ceramide (Fig. 4D), while cells with low SM/ceramide labeling were CD133(-). There were no detectable CD133(+) cells or accumulation of SM and ceramide in normal adjacent liver tissues and age-matched *fro/+* controls, suggesting that accumulation of these two sphingolipids is associated with CSC proliferation or survival in liver.

Increased sphingolipid and neutral lipid synthesis in *fro/fro* liver tumors

Next, we set out to delineate the potential mechanism of increased ceramide synthesis in *fro/fro* liver tumors by measuring the levels of CerSs, especially of those that generate C_{16} -ceramide, which has been shown to exert pro-survival functions (53) and was increased the most in *fro/fro* liver

tumors (Fig. 4B). Two CerSs catalyze C_{16} -ceramide generation, CerS5 and CerS6. RT-PCR and qPCR showed that CerS5 expression was significantly increased when compared with normal adjacent tissues, while CerS6 was below the detection limit (Fig. 5A, B and not shown). These data suggest that CerS5 was distinctly upregulated in *fro/fro* liver tumors, likely to compensate for deficiency of nSMase2.

Alterations of sphingolipid metabolism are often associated with an accumulation of neutral lipids and the formation of LDs in the liver (54). Recent research has found that LD formation contributes to the development of tumors and CSCs (55). To further characterize lipid alterations in the tumor, we visualized hepatic LD content using ORO staining. Liver tissues from young *fro/+* or *fro/fro* mice exhibited little ORO staining (data not shown). Some LD accumulation was observed in *fro/+* liver tissues from aged mice (Fig. 6A), consistent with a previous report that aging increases lipogenesis in the liver (56). Notably, the *fro/fro* liver tumors contained a substantially higher amount of LDs

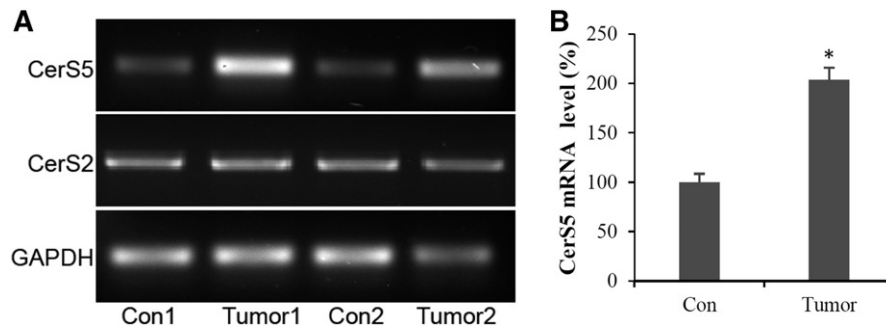


Fig. 5. Aberrant synthesis of sphingolipid in *fro/fro* liver tumors. A: CerS5 was elevated in *fro/fro* tumors shown by RT-PCR using two sets of samples. CerS2 did not change. Controls (Con) were from normal adjacent tissues of *fro/fro* tumors (Tumor). GAPDH was used as loading control. B: CerS5 was elevated in *fro/fro* tumors shown by qPCR. N = 3. * $P < 0.05$.

(Fig. 6C) when compared with the adjacent normal tissue (Fig. 6B) or age-matched controls (Fig. 6A). Interestingly, the non-tumor tissue of the *fro/fro* mice (Fig. 6B) exhibited less ORO staining than that of aged-matched *fro/+* controls (Fig. 6A). Figure 6D shows additional low magnification ORO images of a *fro/fro* liver tumor (encircled by green arrows), which clearly exhibit the profoundly higher ORO staining in *fro/fro* liver tumor when compared with normal adjacent tissues (upper panel and the area outside of green arrow, Fig. 6D). Collectively, these data indicate that the tumors observed in aged *fro/fro* mice are associated with increased lipid accumulation in contrast to the trend observed in non-tumor tissue, where nSMase2 deficiency reduces LD biogenesis.

DISCUSSION

Liver cancer is one of the most fatal and common cancers worldwide. Although in recent years the occurrence of many cancers has decreased, the occurrence rate of liver cancer has steadily increased (57, 58). Liver cancers are usually detected at a late stage and are highly resistant to conventional chemo- and radiotherapy, leading to very poor survival rates.

Genome-wide association studies and genetic analyses have identified that impaired sphingolipid metabolism is common in many cancers, including liver cancer (3, 24, 59, 60). A recent genome-wide methylation analysis and epigenetic unmasking identified nSMase2 (encoded by *Smpd3*) as a tumor suppressor for HCC (24). Overexpression of nSMase2 reduced cell proliferation by 50% in a HCC cell line (24). Conversely, nSMase2 knockdown with small hairpin RNA promoted cell invasion and migration in vitro and increased tumor formation in vivo (24). However, the sphingolipid metabolism affected by nSMase2 and how this altered lipid metabolism regulates tumor formation are not known.

In the current study, liver tumors were observed in over a quarter of aged male *fro/fro* mice (Table 1, Fig. 1). There is no report on tumor formation in nSMase2-deficient animals, most likely because studies on older mice have not been performed. These tumors showed increased proliferation and apoptosis (Fig. 2), a common feature of many malignancies (44, 45). Interestingly, the tumors had an

increased number of CSCs, which was confirmed by Western blot and immunofluorescence labeling of pStat3, a stemness marker (Fig. 3) (34–37). These data indicate that CSCs might be a cell source of the origin of the tumors in *fro/fro* livers.

To study the potentially underlying mechanism, we investigated the sphingolipid metabolism affected by nSMase2 deficiency in the *fro/fro* mice. The *fro/fro* tumors showed a profound increase of SM and ceramide levels (Fig. 4), indicating that nSMase2 deficiency induced a significant sphingolipid makeover specifically in tumor cells and likely CSCs. This assumption is consistent with tumor-specific activation of de novo ceramide and SM synthesis (61), possibly as a compensatory response to the genetic nSMase2 deficiency. Significantly higher levels of ceramides and SM have been reported in breast cancer tissue than in normal tissue (61). SMS2 overexpression promotes mouse liver steatosis, a major contributor to the development of HCC, whereas SMS2 deficiency has the opposite effect (62). Despite a certain level of variation, mounting evidence has demonstrated that sphingolipid metabolism, particularly elevation of SM and ceramide, has essential functions in cancer development (29, 61–66). Importantly, the CSC labeling is concurrent with strong labeling for ceramide and SM (Fig. 4C, D), suggesting that buildup of these two sphingolipids could be a contributing factor for CSC proliferation or survival. This is in line with previous findings that changes in SM and ceramide metabolism associate with CSC maintenance and resistance against apoptosis induction (9, 29, 64).

Expression of CerS5 was distinctly increased in the *fro/fro* liver tumors (Fig. 5), likely accounting for the increase of C_{16} - and dhC_{16} -ceramide levels. Previous studies have shown that palmitate-induced elevation of C_{16} -ceramide promotes LD formation in liver cells (54) and inhibition of de novo ceramide synthesis affects liver lipid metabolism and LD formation in vivo (67), suggesting that an increase of ceramide levels may account for the accumulation of LDs in *fro/fro* tumors (Fig. 6). Aberrant lipid metabolism and LD accumulation are associated with liver tumors (68). While a small side population of CSCs may already show initial alteration of sphingolipid metabolism in normal or precancerous tissue, elevation of SM, CerS5, and ceramide becomes more significant and profound once they grow into a tumor. It is also possible that elevation of SM, CerS5,

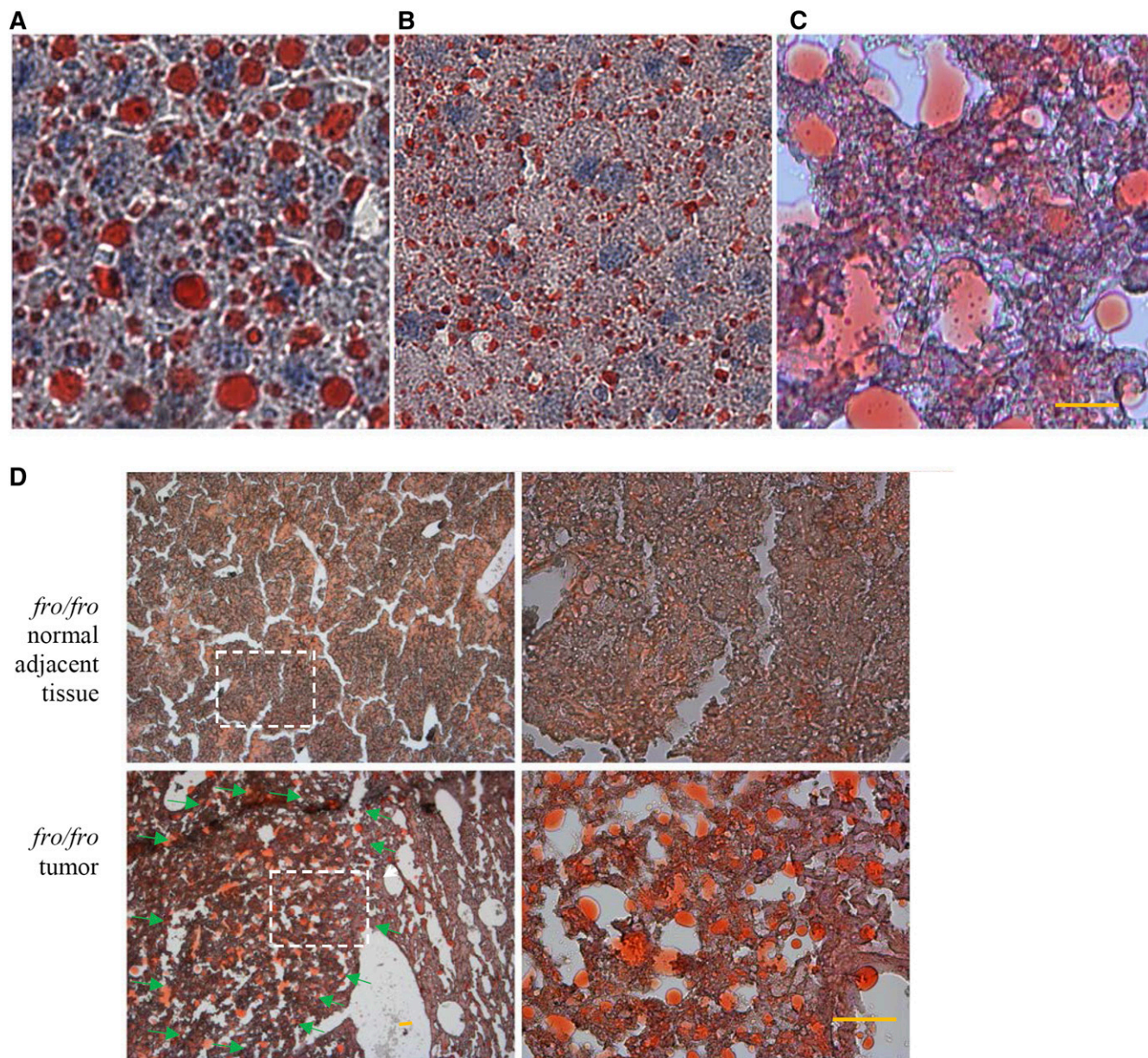



Fig. 6. Aberrant LD accumulation in *fro/fro* liver tumors. A–C: ORO staining of liver lipid LDs in the livers of age-matched *fro/+* control (A), non-tumor *fro/fro* (B), and *fro/fro* liver tumors (C). Scale bars = 5 μm. D: Lower magnification images of ORO staining of *fro/fro* liver tumors and normal adjacent tissues. The area encircled by green arrows is tumor. Scale bars = 20 μm. Insets are shown in the right panels.

and C₁₆-ceramide, accumulation of LDs, and activation of Stat3 lead to dedifferentiation of mature hepatocytes into formation and propagation of CSCs, which then causes tumor formation. These two distinct mechanisms are compatible with accumulation of LDs because of the Warburg effect, a mitochondrial dysfunction preventing fatty acid oxidation in cancer cells (69, 70). This mitochondrial damage leads to a compensatory fermentation and the initiation of dysregulated cell growth, which results in proliferation and propagation of CSCs (69, 71). We will further investigate the mechanistic connection between nSMase2 deficiency, LD formation, and liver tumor growth in future studies.

Another question to be investigated is the gender-specific development of liver tumors in aged male, but not

in female, *fro/fro* mice. This gender-specificity is probably linked to the hypothalamus-pituitary-adrenal axis defect caused by nSMase2 deficiency. There is evidence that HCC is an androgen-sensitive tumor and that sex hormones promote tumor proliferation (72–75). The pituitary gland of the *smpd3* mutant mice showed reduced size, and the numbers of ACTH-positive, FSH- and LH-positive, and other hormone-positive pituicytes were all significantly reduced in the nSMase2-deficient mice (16, 17). In addition, our studies on nSMase2 inhibition and deficiency on plaque formation in Alzheimer's disease clearly showed effects in male, but not in female, mice (76, 77). Hence, gender-specific hormonal effects may underlie the observation that only aged male *fro/fro* mice developed liver tumors. Despite these open questions, our study is the first showing that

nSMase2 deficiency is associated with CSC propagation/survival and liver tumor formation, and will possibly spur future studies to understand the function of sphingolipid metabolism in age-related liver cancer. 

The authors are thankful for the assistance from the Augusta University imaging core facility (director Dr. Paul McNeil) and the sphingolipid core facility at the Medical University of South Carolina (director Dr. Jacek Bielawski). The authors also thank the Department of Neuroscience and Regenerative Medicine (chaired by Dr. Lin Mei), Augusta University, and the Department of Physiology (chaired by Dr. Alan Daugherty), University of Kentucky, for institutional support.

REFERENCES

- Ogretmen, B., and Y. A. Hannun. 2004. Biologically active sphingolipids in cancer pathogenesis and treatment. *Nat. Rev. Cancer*. **4**: 604–616.
- Oskouian, B., and J. D. Saba. 2010. Cancer treatment strategies targeting sphingolipid metabolism. *Adv. Exp. Med. Biol.* **688**: 185–205.
- Pralhada Rao, R., N. Vaidyanathan, M. Rengasamy, A. Mammen Oommen, N. Somaiya, and M. R. Jagannath. 2013. Sphingolipid metabolic pathway: an overview of major roles played in human diseases. *J. Lipids*. **2013**: 178910.
- Proia, R. L., and T. Hla. 2015. Emerging biology of sphingosine-1-phosphate: its role in pathogenesis and therapy. *J. Clin. Invest.* **125**: 1379–1387.
- Nagahashi, M., Y. Matsuda, K. Moro, J. Tsuchida, D. Soma, Y. Hirose, T. Kobayashi, S. Kosugi, K. Takabe, M. Komatsu, et al. 2016. DNA damage response and sphingolipid signaling in liver diseases. *Surg. Today*. **46**: 995–1005.
- Dubois, N., E. Rio, N. Ripoche, V. Ferchaud-Roucher, M. H. Gaugler, L. Campion, M. Krempf, C. Carrie, M. Mahe, X. Mirabel, et al. 2016. Plasma ceramide, a real-time predictive marker of pulmonary and hepatic metastases response to stereotactic body radiation therapy combined with irinotecan. *Radiother. Oncol.* **119**: 229–235.
- Krishnamurthy, K., G. Wang, D. Rokhfeld, and E. Bieberich. 2008. Deoxycholate promotes survival of breast cancer cells by reducing the level of pro-apoptotic ceramide. *Breast Cancer Res.* **10**: R106.
- Bradley, E., S. Dasgupta, X. Jiang, X. Zhao, G. Zhu, Q. He, M. Dinkins, E. Bieberich, and G. Wang. 2014. Critical role of spns2, a sphingosine-1-phosphate transporter, in lung cancer cell survival and migration. *PLoS One*. **9**: e110119.
- Kong, J. N., Q. He, G. Wang, S. Dasgupta, M. B. Dinkins, G. Zhu, A. Kim, S. Spassieva, and E. Bieberich. 2015. Guggulsterone and bexarotene induce secretion of exosome-associated breast cancer resistance protein and reduce doxorubicin resistance in MDA-MB-231 cells. *Int. J. Cancer*. **137**: 1610–1620.
- Ordoñez, R., A. Fernández, N. Prieto-Domínguez, L. Martínez, C. García-Ruiz, J. C. Fernández-Checa, J. L. Mauriz, and J. González-Gallego. 2015. Ceramide metabolism regulates autophagy and apoptotic cell death induced by melatonin in liver cancer cells. *J. Pineal Res.* **59**: 178–189.
- Nagahashi, M., K. Yuza, Y. Hirose, M. Nakajima, R. Ramanathan, N. C. Hait, P. B. Hylemon, H. Zhou, K. Takabe, and T. Wakai. 2016. The roles of bile acids and sphingosine-1-phosphate signaling in the hepatobiliary diseases. *J. Lipid Res.* **57**: 1636–1643.
- Airola, M. V., and Y. A. Hannun. 2013. Sphingolipid metabolism and neutral sphingomyelinases. *Handb. Exp. Pharmacol.* **215**: 57–76.
- Hannun, Y. A., and L. M. Obeid. 2008. Principles of bioactive lipid signalling: lessons from sphingolipids. *Nat. Rev. Mol. Cell Biol.* **9**: 139–150.
- Hannun, Y. A. 1994. The sphingomyelin cycle and the second messenger function of ceramide. *J. Biol. Chem.* **269**: 3125–3128.
- Shamseddine, A. A., M. V. Airola, and Y. A. Hannun. 2015. Roles and regulation of neutral sphingomyelinase-2 in cellular and pathological processes. *Adv. Biol. Regul.* **57**: 24–41.
- Stoffel, W., B. Jenke, B. Block, M. Zumbansen, and J. Koebke. 2005. Neutral sphingomyelinase 2 (smpd3) in the control of postnatal growth and development. *Proc. Natl. Acad. Sci. USA*. **102**: 4554–4559.
- Stoffel, W., B. Jenke, B. Holz, E. Binczek, R. H. Gunter, J. Knifka, J. Koebke, and A. Niehoff. 2007. Neutral sphingomyelinase (SMPD3) deficiency causes a novel form of chondrodysplasia and dwarfism that is rescued by Col2A1-driven smpd3 transgene expression. *Am. J. Pathol.* **171**: 153–161.
- Stoffel, W., I. Hammels, B. Jenke, E. Binczek, I. Schmidt-Soltan, S. Brodesser, A. Schauss, J. Etich, J. Heilig, and F. Zaucke. 2016. Neutral sphingomyelinase (SMPD3) deficiency disrupts the Golgi secretory pathway and causes growth inhibition. *Cell Death Dis.* **7**: e2488.
- Schuchman, E. H., and M. P. Wasserstein. 2015. Types A and B Niemann-Pick disease. *Best Pract. Res. Clin. Endocrinol. Metab.* **29**: 237–247.
- Schuchman, E. H., and M. P. Wasserstein. 2016. Types A and B Niemann-Pick disease. *Pediatr. Endocrinol. Rev.* **13** (Suppl. 1): 674–681.
- Clarke, C. J., B. X. Wu, and Y. A. Hannun. 2011. The neutral sphingomyelinase family: identifying biochemical connections. *Adv. Enzyme Regul.* **51**: 51–58.
- Kim, W. J., R. A. Okimoto, L. E. Purton, M. Goodwin, S. M. Haserlat, F. Dayyani, D. A. Sweetser, A. I. McClatchey, O. A. Bernard, A. T. Look, et al. 2008. Mutations in the neutral sphingomyelinase gene SMPD3 implicate the ceramide pathway in human leukemias. *Blood*. **111**: 4716–4722.
- Bhati, R., C. Patterson, C. A. Livasy, C. Fan, D. Ketelsen, Z. Hu, E. Reynolds, C. Tanner, D. T. Moore, F. Gabrielli, et al. 2008. Molecular characterization of human breast tumor vascular cells. *Am. J. Pathol.* **172**: 1381–1390.
- Revill, K., T. Wang, A. Lachenmayer, K. Kojima, A. Harrington, J. Li, Y. Hoshida, J. M. Llovet, and S. Powers. 2013. Genome-wide methylation analysis and epigenetic unmasking identify tumor suppressor genes in hepatocellular carcinoma. *Gastroenterology*. **145**: 1424–1435. e1–25.
- Spassieva, S., and E. Bieberich. 2011. The gut-to-breast connection - interdependence of sterols and sphingolipids in multidrug resistance and breast cancer therapy. *Anticancer. Agents Med. Chem.* **11**: 882–890.
- Bieberich, E., J. Silva, G. Wang, K. Krishnamurthy, and B. G. Condie. 2004. Selective apoptosis of pluripotent mouse and human stem cells by novel ceramide analogues prevents teratoma formation and enriches for neural precursors in ES cell-derived neural transplants. *J. Cell Biol.* **167**: 723–734.
- Bieberich, E. 2011. Ceramide in stem cell differentiation and embryo development: novel functions of a topological cell-signaling lipid and the concept of ceramide compartments. *J. Lipids*. **2011**: 610306.
- Bieberich, E. 2012. Ceramide and sphingosine-1-phosphate signaling in embryonic stem cell differentiation. *Methods Mol. Biol.* **874**: 177–192.
- Gupta, V., K. N. Bhingre, S. B. Hosain, K. Xiong, X. Gu, R. Shi, M. Y. Ho, K. H. Khoo, S. C. Li, Y. T. Li, et al. 2012. Ceramide glycosylation by glucosylceramide synthase selectively maintains the properties of breast cancer stem cells. *J. Biol. Chem.* **287**: 37195–37205.
- Yamashita, T., and X. W. Wang. 2013. Cancer stem cells in the development of liver cancer. *J. Clin. Invest.* **123**: 1911–1918.
- Yamashita, T., and S. Kaneko. 2014. Orchestration of hepatocellular carcinoma development by diverse liver cancer stem cells. *J. Gastroenterol.* **49**: 1105–1110.
- Shackleton, M., E. Quintana, E. R. Fearon, and S. J. Morrison. 2009. Heterogeneity in cancer: cancer stem cells versus clonal evolution. *Cell*. **138**: 822–829.
- Wolf, B., K. Krieg, C. Falk, K. Breuhahn, H. Keppeler, T. Biedermann, E. Schmid, S. Warmann, J. Fuchs, S. Vetter, et al. 2016. Inducing differentiation of premalignant hepatic cells as a novel therapeutic strategy in hepatocarcinoma. *Cancer Res.* **76**: 5550–5561.
- Niwa, H., T. Burdon, I. Chambers, and A. Smith. 1998. Self-renewal of pluripotent embryonic stem cells is mediated via activation of STAT3. *Genes Dev.* **12**: 2048–2060.
- Ghoshal, S., B. C. Fuchs, and K. K. Tanabe. 2016. STAT3 is a key transcriptional regulator of cancer stem cell marker CD133 in HCC. *Hepatobiliary Surg. Nutr.* **5**: 201–203.
- Won, C., B. H. Kim, E. H. Yi, K. J. Choi, E. K. Kim, J. M. Jeong, J. H. Lee, J. J. Jang, J. H. Yoon, W. I. Jeong, et al. 2015. Signal transducer and activator of transcription 3-mediated CD133 up-regulation

- contributes to promotion of hepatocellular carcinoma. *Hepatology*. **62**: 1160–1173.
37. Bradley, E., E. Bieberich, N. F. Mivechi, D. Tangpisuthipongsa, and G. Wang. 2012. Regulation of embryonic stem cell pluripotency by heat shock protein 90. *Stem Cells*. **30**: 1624–1633.
 38. Aubin, I., C. P. Adams, S. Opsahl, D. Septier, C. E. Bishop, N. Auge, R. Salvayre, A. Negre-Salvayre, M. Goldberg, J. L. Guenet, et al. 2005. A deletion in the gene encoding sphingomyelin phosphodiesterase 3 (Smpd3) results in osteogenesis and dentinogenesis imperfecta in the mouse. *Nat. Genet.* **37**: 803–805.
 39. Wang, G., M. Dinkins, Q. He, G. Zhu, C. Poirier, A. Campbell, M. Mayer-Proschel, and E. Bieberich. 2012. Astrocytes secrete exosomes enriched with proapoptotic ceramide and prostate apoptosis response 4 (PAR-4): potential mechanism of apoptosis induction in Alzheimer disease (AD). *J. Biol. Chem.* **287**: 21384–21395.
 40. Guenet, J. L., R. Stanescu, P. Maroteaux, and V. Stanescu. 1981. Fragilitas ossium: a new autosomal recessive mutation in the mouse. *J. Hered.* **72**: 440–441.
 41. Krishnamurthy, K., S. Dasgupta, and E. Bieberich. 2007. Development and characterization of a novel anti-ceramide antibody. *J. Lipid Res.* **48**: 968–975.
 42. Bielawski, J., Z. M. Szulc, Y. A. Hannun, and A. Bielawska. 2006. Simultaneous quantitative analysis of bioactive sphingolipids by high-performance liquid chromatography-tandem mass spectrometry. *Methods*. **39**: 82–91.
 43. Fabregat, I., C. Roncero, and M. Fernandez. 2007. Survival and apoptosis: a dysregulated balance in liver cancer. *Liver Int.* **27**: 155–162.
 44. Al-Ejeh, F., J. M. Darby, K. Pensa, K. R. Diener, J. D. Hayball, and M. P. Brown. 2007. In vivo targeting of dead tumor cells in a murine tumor model using a monoclonal antibody specific for the La autoantigen. *Clin. Cancer Res.* **13**: 5519s–5527s.
 45. Wyllie, A. H., J. F. Kerr, and A. R. Currie. 1980. Cell death: the significance of apoptosis. *Int. Rev. Cytol.* **68**: 251–306.
 46. Taub, R. 2004. Liver regeneration: from myth to mechanism. *Nat. Rev. Mol. Cell Biol.* **5**: 836–847.
 47. Machida, K. 2017. Existence of cancer stem cells in hepatocellular carcinoma: myth or reality? *Hepatol. Int.* **11**: 143–147.
 48. Zheng, Y. W., T. Tsuchida, T. Shima, B. Li, T. Takebe, R. R. Zhang, Y. Sakurai, Y. Ueno, K. Sekine, N. Ishibashi, et al. 2014. The CD133+CD44+ precancerous subpopulation of oval cells is a therapeutic target for hepatocellular carcinoma. *Stem Cells Dev.* **23**: 2237–2249.
 49. Newton, J., S. Lima, M. Maceyka, and S. Spiegel. 2015. Revisiting the sphingolipid rheostat: Evolving concepts in cancer therapy. *Exp. Cell Res.* **333**: 195–200.
 50. Furuya, H., Y. Shimizu, and T. Kawamori. 2011. Sphingolipids in cancer. *Cancer Metastasis Rev.* **30**: 567–576.
 51. García-Barros, M., N. Coant, J. P. Truman, A. J. Snider, and Y. A. Hannun. 2014. Sphingolipids in colon cancer. *Biochim. Biophys. Acta.* **1841**: 773–782.
 52. Qin, J., E. Berdyshev, C. Poirer, N. B. Schwartz, and G. Dawson. 2012. Neutral sphingomyelinase 2 deficiency increases hyaluronan synthesis by up-regulation of Hyaluronan synthase 2 through decreased ceramide production and activation of Akt. *J. Biol. Chem.* **287**: 13620–13632.
 53. Senkal, C. E., S. Ponnusamy, J. Bielawski, Y. A. Hannun, and B. Ogretmen. 2010. Antiapoptotic roles of ceramide-synthase-6-generated C16-ceramide via selective regulation of the ATF6/CHOP arm of ER-stress-response pathways. *FASEB J.* **24**: 296–308.
 54. Deevska, G. M., and M. N. Nikolova-Karakashian. 2017. The expanding role of sphingolipids in lipid droplet biogenesis. *Biochim. Biophys. Acta.* **1862**: 1155–1165.
 55. Tirinato, L., F. Pagliari, T. Limongi, M. Marini, A. Falqui, J. Seco, P. Candeloro, C. Liberale, and E. Di Fabrizio. 2017. An overview of lipid droplets in cancer and cancer stem cells. *Stem Cells Int.* **2017**: 1656053.
 56. Gong, Z., E. Tas, S. Yakar, and R. Muzumdar. 2017. Hepatic lipid metabolism and non-alcoholic fatty liver disease in aging. *Mol. Cell. Endocrinol.* **455**: 115–130.
 57. Rao, C. V., A. S. Asch, and H. Y. Yamada. 2017. Frequently mutated genes/pathways and genomic instability as prevention targets in liver cancer. *Carcinogenesis*. **38**: 2–11.
 58. Endig, J., L. E. Buitrago-Molina, S. Marhenke, F. Reisinger, A. Saborowski, J. Schutt, F. Limbourg, C. Konecke, A. Schreder, A. Michael, et al. 2016. Dual role of the adaptive immune system in liver injury and hepatocellular carcinoma development. *Cancer Cell*. **30**: 308–323.
 59. Ponnusamy, S., M. Meyers-Needham, C. E. Senkal, S. A. Saddoughi, D. Sentelle, S. P. Selvam, A. Salas, and B. Ogretmen. 2010. Sphingolipids and cancer: ceramide and sphingosine-1-phosphate in the regulation of cell death and drug resistance. *Future Oncol.* **6**: 1603–1624.
 60. Chen, Y., Z. Ma, L. Min, H. Li, B. Wang, J. Zhong, and L. Dai. 2015. Biomarker identification and pathway analysis by serum metabolomics of lung cancer. *BioMed Res. Int.* **2015**: 183624.
 61. Nagahashi, M., J. Tsuchida, K. Moro, M. Hasegawa, K. Tatsuda, I. A. Woelfel, K. Takabe, and T. Wakai. 2016. High levels of sphingolipids in human breast cancer. *J. Surg. Res.* **204**: 435–444.
 62. Li, Y., J. Dong, T. Ding, M. S. Kuo, G. Cao, X. C. Jiang, and Z. Li. 2013. Sphingomyelin synthase 2 activity and liver steatosis: an effect of ceramide-mediated peroxisome proliferator-activated receptor gamma2 suppression. *Arterioscler. Thromb. Vasc. Biol.* **33**: 1513–1520.
 63. Xu, J. X., E. Morii, Y. Liu, N. Nakamichi, J. Ikeda, H. Kimura, and K. Aozasa. 2007. High tolerance to apoptotic stimuli induced by serum depletion and ceramide in side-population cells: high expression of CD55 as a novel character for side-population. *Exp. Cell Res.* **313**: 1877–1885.
 64. Liu, Y. Y., R. A. Hill, and Y. T. Li. 2013. Ceramide glycosylation catalyzed by glucosylceramide synthase and cancer drug resistance. *Adv. Cancer Res.* **117**: 59–89.
 65. Pewzner-Jung, Y., O. Brenner, S. Braun, E. L. Laviad, S. Ben-Dor, E. Feldmesser, S. Horn-Saban, D. Amann-Zalcenstein, C. Raanan, T. Berkutzi, et al. 2010. A critical role for ceramide synthase 2 in liver homeostasis: II. insights into molecular changes leading to hepatopathy. *J. Biol. Chem.* **285**: 10911–10923.
 66. Pewzner-Jung, Y., H. Park, E. L. Laviad, L. C. Silva, S. Lahiri, J. Stiban, R. Erez-Roman, B. Brugger, T. Sachsenheimer, F. Wieland, et al. 2010. A critical role for ceramide synthase 2 in liver homeostasis: I. alterations in lipid metabolic pathways. *J. Biol. Chem.* **285**: 10902–10910.
 67. Kurek, K., P. Wiesiolek-Kurek, D. M. Piotrowska, B. Lukaszuk, A. Chabowski, and M. Zendzianendzian-Piotrowska. 2014. Inhibition of ceramide de novo synthesis with myricin affects lipid metabolism in the liver of rats with streptozotocin-induced type 1 diabetes. *BioMed Res. Int.* **2014**: 980815.
 68. Bechmann, L. P., R. A. Hannivoort, G. Gerken, G. S. Hotamisligil, M. Trauner, and A. Canbay. 2012. The interaction of hepatic lipid and glucose metabolism in liver diseases. *J. Hepatol.* **56**: 952–964.
 69. Seyfried, T. N. 2015. Cancer as a mitochondrial metabolic disease. *Front. Cell Dev. Biol.* **3**: 43.
 70. Liberti, M. V., and J. W. Locasale. 2016. The Warburg effect: how does it benefit cancer cells? *Trends Biochem. Sci.* **41**: 211–218.
 71. Pacini, N., and F. Borziani. 2014. Cancer stem cell theory and the Warburg effect, two sides of the same coin? *Int. J. Mol. Sci.* **15**: 8893–8930.
 72. Guy, J., and M. G. Peters. 2013. Liver disease in women: the influence of gender on epidemiology, natural history, and patient outcomes. *Gastroenterol. Hepatol. (N. Y.)*. **9**: 633–639.
 73. Matsumoto, T., H. Takagi, and M. Mori. 2000. Androgen dependency of hepatocarcinogenesis in TGFalpha transgenic mice. *Liver*. **20**: 228–233.
 74. Tanaka, K., H. Sakai, M. Hashizume, and T. Hirohata. 2000. Serum testosterone:estradiol ratio and the development of hepatocellular carcinoma among male cirrhotic patients. *Cancer Res.* **60**: 5106–5110.
 75. Naugler, W. E., T. Sakurai, S. Kim, S. Maeda, K. Kim, A. M. Elsharkawy, and M. Karin. 2007. Gender disparity in liver cancer due to sex differences in MyD88-dependent IL-6 production. *Science*. **317**: 121–124.
 76. Dinkins, M. B., S. Dasgupta, G. Wang, G. Zhu, and E. Bieberich. 2014. Exosome reduction in vivo is associated with lower amyloid plaque load in the 5XFAD mouse model of Alzheimer's disease. *Neurobiol. Aging*. **35**: 1792–1800.
 77. Dinkins, M. B., J. Enasko, C. Hernandez, G. Wang, J. Kong, I. Helwa, Y. Liu, A. V. Terry, Jr., and E. Bieberich. 2016. Neutral sphingomyelinase-2 deficiency ameliorates Alzheimer's disease pathology and improves cognition in the 5XFAD mouse. *J. Neurosci.* **36**: 8653–8667.